AFAL-TR-79-1114

CHAFF RADAR CROSS SECTION STUDIES AND CALCULATIONS

The Ohio State University
ElectroScience Laboratory
Department of Electrical Engineering
Columbus, Ohio 43212

May 1978

TECHNICAL REPORT AFAL-TR-79-1114

Interim Report for Period 1 January 1976 - 30 June 1977

AIR FORCE AVIONICS LABORATORY
AIR FORCE WRIGHT AERONAUTICAL LABORATORIES
AIR FORCE SYSTEMS COMMAND
WRIGHT-PATTERSON AIR FORCE BASE, OHIO 45433

NOTICE

When Government drawings, specifications, or other data are used for any purpose other than in connection with a definitely related Government procurement operation, the United States Government thereby incurs no responsibility nor any obligation whatsoever; and the fact that the government may have formulated, furnished, or in any way supplied the said drawings, specifications, or other data, is not to be regarded by implication or otherwise as in any manner licensing the holder or any other person or corporation, or conveying any rights or permission to manufacture, use, or sell any patented invention that may in any way be related thereto.

This report has been reviewed by the Information Office (OI) and is releasable to the National Technical Information Service (NTIS). At NTIS, it will be available to the general public, including foreign nations.

This technical report has been reviewed and is approved for publication.

ROBERT J. PUSKAR
Elec Engr, Observables Gp
Passive ECM Branch
Electronic Warfare Division

WILLIAM F. BAHRET
Chief, Passive ECM Branch
Electronic Warfare Division

FOR THE COMMANDER

JOSEPH H. JACOBS, Colonel, USAF
Chief, Electronic Warfare Division
Air Force Avionics Laboratory

"If your address has changed, if you wish to be removed from our mailing list, or if the addressee is no longer employed by your organization please notify AFAL/WRP-3, W-PAFB, OH 45433 to help us maintain a current mailing list".

Copies of this report should not be returned unless return is required by security considerations, contractual obligations, or notice on a specific document.

SECURITY CLASSIFICATION OF THIS PAGE (When Data Entered)

REPORT DOCUMENTATION PAGE	READ INSTRUCTIONS BEFORE COMPLETING FORM
1. REPORT NUMBER: AFAL-TR-79-1114	2. GOVT ACCESSION NO.	3. RECIPIENT'S CATALOG NUMBER
4. TITLE (and Subtitle): CHAFF RADAR CROSS SECTION STUDIES AND CALCULATIONS	5. TYPE OF REPORT & PERIOD COVERED: Interim Report 1 Jan 76 – 30 Jun 77
	6. PERFORMING ORG. REPORT NUMBER: ESL-784346-7
7. AUTHOR(s): R. J. Garbacz	8. CONTRACT OR GRANT NUMBER(s): Contract F33615-76-C-1024
9. PERFORMING ORGANIZATION NAME AND ADDRESS: The Ohio State University ElectroScience Laboratory, Department of Electrical Engineering, Columbus, Ohio 43212	10. PROGRAM ELEMENT, PROJECT, TASK AREA & WORK UNIT NUMBERS: Project 76331328
11. CONTROLLING OFFICE NAME AND ADDRESS: Air Force Avionics Laboratory (AFAL/WRP), Air Force Wright Aeronautical Laboratories, Wright-Patterson Air Force Base, Ohio 45433	12. REPORT DATE: May 1978
	13. NUMBER OF PAGES: 36
14. MONITORING AGENCY NAME & ADDRESS (if different from Controlling Office)	15. SECURITY CLASS. (of this report): Unclassified
	15a. DECLASSIFICATION/DOWNGRADING SCHEDULE

16. DISTRIBUTION STATEMENT (of this Report)

Approved for public release; distribution unlimited.

17. DISTRIBUTION STATEMENT (of the abstract entered in Block 20, if different from Report)

18. SUPPLEMENTARY NOTES

19. KEY WORDS (Continue on reverse side if necessary and identify by block number)

Chaff
Scattering
Dipole
Wire

20. ABSTRACT (Continue on reverse side if necessary and identify by block number)

The objective of Contract F33615-76-C-1024 has been to analytically and experimentally investigate chaff scattering and the reduction of antenna-related radar cross section. This final report summarizes results obtained during the interim 1 January 1976 through 30 June 1977 on the chaff aspect of the effort. Included are summaries of 1) an investigation of scattering by a long wire excited by either a plane wave or by a nearby short dipole with sinusoidal current distribution and 2) an experimental study of small foam shapes very densely coated with chaff filaments.

DD FORM 1 JAN 73 1473 EDITION OF 1 NOV 65 IS OBSOLETE

SECURITY CLASSIFICATION OF THIS PAGE (When Data Entered)

TABLE OF CONTENTS

LIST OF ILLUSTRATIONS

LIST OF ILLUSTRATIONS (CON'T)

SECTION I
INTRODUCTION

Efficient use of chaff for the protection of aircraft in tactical situations demands knowledge of the radar scattering characteristics of small, dense clouds of dipoles. In extreme cases, just after ejection from the vehicle into the wind stream, dipole densities of thousands per cubic wavelength are encountered. Moments later, lower densities on the order of a hundred dipoles per cubic wavelength are encountered. Either case presents problems not addressed in our previous work (1). In that effort, the method of moments technique, whereby the electromagnetic boundary-value problem is cast in a matrix formulation, has been used to obtain the induced dipole currents and scattering cross sections of clouds with dipole densities up to about eight per wavelength. Greater densities were investigated and it was found that the closer spacings between dipoles in such clouds demanded a representation of each dipole current in more than two piecewise sinusoidal segments, thereby requiring the inversion of larger matrices. The resulting increase in time and computer memory is a severe limitation of the method of moments approach.

Furthermore, our past work was devoted almost exclusively to chaff elements which were one half wavelength long, i.e., which exhibited a high resonant radar return. Chaff units, however, commonly contain dipoles of several lengths to meet radar threats at several selected frequencies. The low frequencies present no new problems, but at the higher frequencies, those dipoles designed to be resonant at low frequencies become electrically long, and require many piecewise sinusoidal modes to adequately describe the induced currents. This enlarges the matrix to sizes which cannot be accommodated by computers.

Thus, two extensions of our work were required. These are 1) analysis of electrically longer chaff elements and 2) analysis of chaff elements which are more densely packed. In this report, we summarize efforts directed at these two aspects of the chaff problem.

SECTION II
TRAVELING-WAVE THEORY FOR THE LONG FINITE WIRE

A. Introductory Remarks

In order to accommodate electrically long chaff elements in a computer model of a chaff cloud, a mathematical model had to be devised which accurately predicts the current induced on a long, linear filament due to plane wave excitation, or due to excitation by a nearby dipole. The nearby dipole could be considered as another shorter member of the chaff cloud, or as a segment of another long filament in the cloud. In any case, it was desired that the determination of the current on the long filament be accomplished with the fewest number of unknowns so that ultimately the matrix representation of the chaff cloud be as small as possible. In this section we develop a representation for the current on a long thin wire with finite conductivity in terms of three travelling wave modes, far fewer modes than would be demanded by the standard method of moments technique. In fact, this travelling wave model becomes more accurate as the wire grows longer.

Let $Y_i(z)$ denote the current distribution on an infinitely-long wire driven with a one-volt generator at the origin. Also let $Y(z,z')$ denote the current at z on a finite wire driven with a one-volt generator at z'. Hallen (2) developed expressions for $Y(z,z')$ in terms of $Y_i(z)$ and equivalent generators at the end of the wire. Later several others (3,4,5) contributed to this formulation. L. C. Shen (6) extended the technique to the plane-wave scattering problem.

The admittance function $Y(z,z')$ may be considered a Green's function for the finite wire in the sense that it determines the response $I(z)$ to an arbitrary excitation as follows:

$$I(z) = \int_{-d}^{d} E_z^i(0,z')\, Y(z,z')\, dz' \qquad (1)$$

where $I(z)$ denotes the current distribution on the wire and $E_z^i(0,z)$ denotes the incident electric field intensity evaluated on the axis of the wire. This relation was presented by Jordan (7) and Schelkunoff and Friis (8) and has been used by others (9).

These techniques have been employed only for the admittance and plane-wave response of perfectly conducting wires. This report extends the techniques to imperfectly-conducting wires and near-zone scattering problems. We consider the near-zone time-harmonic situation with the time dependence $e^{j\omega t}$ understood. The exterior medium is considered to be free space with parameters μ_o and ε_o.

B. The Admittance of the Infinitely-long Wire

For the infinitely-long wire, the counterpart of Equation (1) is

$$I(z) = \int_{-\infty}^{\infty} E_z^i(0,z')\, Y_i(z-z')\, dz' \ . \qquad (2)$$

It is not difficult to solve for the current I(z) induced on the infinite wire when $E_z^i(0,z) = E_o e^{jhz}$ or when $E_z^i(0,z) = V_o \delta(z)$. By comparing these known solutions with Equation (2), we find

$$Y_l(z) = (jk/\eta) \int_{-\infty}^{\infty} \frac{e^{-jhz}\, dh}{\alpha[\alpha K_o(\alpha a) + j\omega\epsilon_o Z_s(\alpha a)]} \tag{3}$$

$$\alpha^2 = h^2 - k^2 \tag{4}$$

where $k = \omega\sqrt{\mu_o \epsilon_o}$ and $\eta = \sqrt{\mu_o/\epsilon_o}$. The wire radius is denoted by "a", and the surface impedance Z_s of the wire is a known function* of h.

C. Traveling-wave Theory for Admittance of Finite Antenna

As shown in Figure 1, we let ℓ denote the wire length, $d = \ell/2$, and z measures position along the wire from an origin at the center.

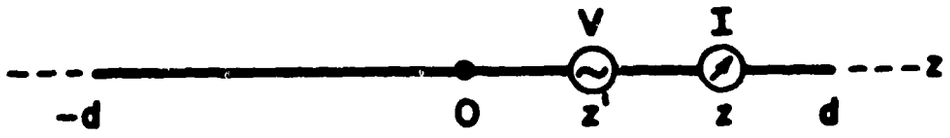

Figure 1. The Admittance Function Y(z,z') for a Cylindrical-wire Antenna is Defined by Inserting a Unit Voltage Generator at z' and Measuring the Current with an Ammeter at z.

For a finite wire, Equation (1) is not considered a rigorous relation. Nevertheless, it is very useful in thin-wire applications. Equation (1) could probably be made rigorous by extending the limits to infinity and letting the resulting expression define the function Y(z,z'). Then Y(z,z') might become small but would not vanish when z and/or z' moved beyond the endpoints of the wire.

*Even when the surface impedance vanishes, Equation (3) differs from the admittance function investigated by Hallen (2), corresponding to delta-gap excitation.

When a unit voltage generator is inserted at z' on a finite antenna, the following "equivalent circuit" has been suggested (2) for the current distribution Y(z,z'). On the corresponding infinite antenna, insert a unit voltage generator at z'. To generate traveling waves of current similar to those reflected from the ends of the finite antenna, insert a generator V_1 at z = -d and another generator V_2 at z = d in the infinite antenna. Now if V_1 and V_2 are suitably adjusted, the resulting current distribution on the infinite antenna is considered to be an approximation for the admittance Y(z,z') of the finite antenna in the range -d< z< d. Beyond this range, the current on the infinite antenna is not considered to have physical significance. We propose the name "traveling-wave theory" for this simple model of the finite antenna.

According to the traveling-wave theory, the admittance function for the finite antenna is given approximately by (2,3,4,5)

$$Y(z,z') = Y_i(z-z') + (A/D)\, Y_i(d+z) + (B/D)\, Y_i(d-z) \tag{5}$$

$$A = R_o \left[Y_i(d+z') + R_o\, Y_i(\ell)\, Y_i(d-z')\right] \tag{6}$$

$$B = R_o \left[Y_i(d-z') + R_o\, Y_i(\ell)\, Y_i(d+z')\right] \tag{7}$$

$$R_o = (\eta/\pi) \left[\ln(\gamma ka) + j\, \pi/2\right] \tag{8}$$

$$D = 1 - R_o^2\, Y_i^2(\ell) \tag{9}$$

where $\gamma = 1.781$. The first term in Equation (5) represents the current wave traveling outward from the generator at z'. The second and third terms represent waves traveling outward from the equivalent generators at -d and +d respectively. If Equation (5) is employed to calculate the Green's function for use in Equation (1), the first term $Y_i(z-z')$ is defined by Equation (3). However, when Equation (5) is used to calculate the current distribution on a transmitting antenna, the first term should be defined to correspond with the gap-region geometry on the real antenna.

For the last two terms in Equation (5), and for Equations (6-9), the most appropriate definition of $Y_i(z)$ is less clear. For thin wires, however, good results are obtained by using Equation (3). One suggestion is to define Y_i in such a way as to achieve the appropriate edge condition at the ends of the wire.

Equation (8) for R_o is presented in the literature (3,5) for perfectly conducting wires. We have found this expression to be suitable also for imperfectly-conducting thin wires if the radius "a" is equal to or greater than the skin depth. Anderson (1) points out that the quantity R_o is dependent on the shape of the end regions of the wire (i.e., flat or hemispherical endcaps) and shows how R_o can be determined empirically from experimental measurements.

D. Traveling-wave Theory for Plane-wave Incident on Finite wire

When a theta-polarized plane wave is incident on a straight wire with infinite length, the current induced on the wire is given by

$$I(z) = I_o\, e^{jhz} \tag{10}$$

where $h = k \cos\theta$. When this plane wave is incident on a finite wire as in Figure 2, traveling-wave theory gives the following approximation for the induced current distribution (6):

$$I(z) = I_o[e^{jhz} + (F/D)\, Y_i(d+z) + (G/D)\, Y_i(d-z)] \tag{11}$$

$$F = F(\theta)\, e^{-jhd} + R_o\, R(\alpha)\, Y_i(\ell)\, e^{jhd} \tag{12}$$

$$G = R(\alpha)\, e^{jhd} + R_o\, R(\alpha)\, Y_i(\ell)\, e^{-jhd} \tag{13}$$

$$R(\theta) = (\eta/\pi)\, \{\ell n\, [\gamma ka \cos(\theta/2)] + j\, \pi/2\} \tag{14}$$

where $\alpha = \pi - \theta$ and R_o and D are given by Equations (8) and (9). Equation (14) for $R(\theta)$ is presented in the literature (6) for a perfectly conducting wire, and a refinement has been presented (10) for near-grazing incidence. We have found Equation (14) to be suitable also for imperfectly-conducting thin wires when the radius "a" is equal to or greater than the skin depth.

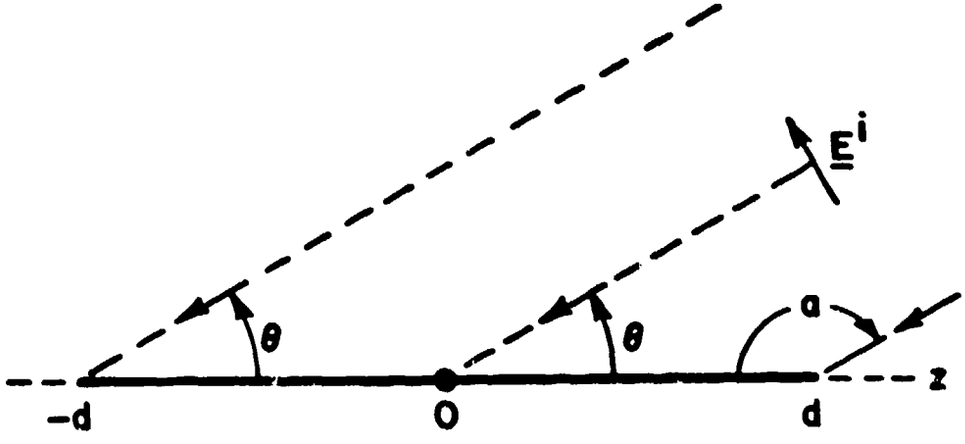

Figure 2. A Theta-polarized Plane Wave Incident on a Straight Wire with Length $\ell = 2d$.

Of course, the current I(z) induced by a plane wave can also be determined from Equations (1) and (5-9) without recourse to the function $R(\theta)$.

E. Green's-Function Technique for Near-Zone Scattering

Consider the situation illustrated in Figure 3 where a sinusoidal electric dipole radiates in the presence of a straight wire. In general the source may be a sinusoidal V-dipole with unequal arm lengths, and the dipole and the wire need not be coplanar. The current induced on the wire is given by Equation (1) where E_z^i denotes the free-space field of the dipole and $Y(z,z')$ is given by Equations (5-9). Equations (11-14) are not applicable to this problem unless one expands the incident field in a spectrum of plane waves.

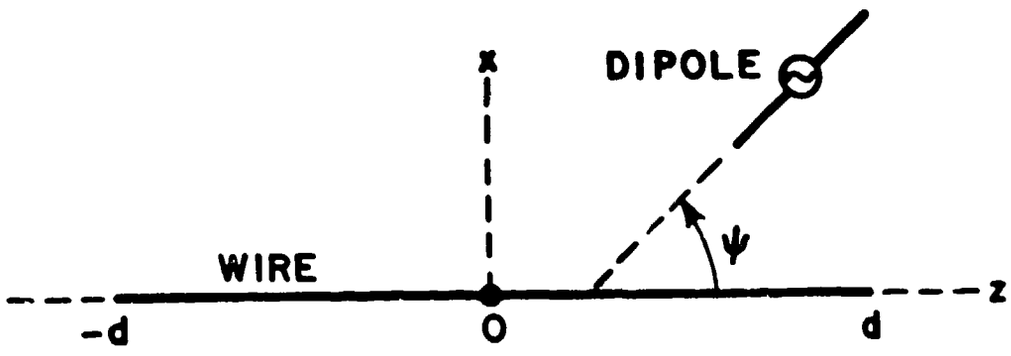

Figure 3. A Sinusoidal Electric Dipole Radiates in the Presence of a Nearby Straight Wire.

The function $Y(z,z')$ is continuous, although it has a slope discontinuity at z'. Furthermore, we may consider $Y(z,z')$ to vanish at both ends of the wire. Thus it is appropriate to interpolate this function with subsectional sinusoidal basis as follows:

$$Y(z,z') = \sum_{1}^{N} \frac{Y(z,z_n)\, P_n(z') \sin k(s - |z'-z_n|)}{\sin(ks)} \tag{15}$$

$$s = \ell/(N+1) \tag{16}$$

$$z_n = -d + ns \tag{17}$$

$$P_n(z') = \begin{cases} 1, & z_n - s < z' < z_n + s \\ 0, & \text{elsewhere} \end{cases} \tag{18}$$

From Equations (1) and (15-18),

$$I(z) = -I_o \sum_1^N Y(z,z_n) Z_{on} \tag{19}$$

$$Z_{on} = \frac{-1}{I_o \sin(ks)} \int_{z_n - s}^{z_n + s} E_z^i(0,z') \sin k(s - |z' - z_n|)\, dz' \tag{20}$$

where I_o denotes the terminal current of the sinusoidal dipole.

Equation (20) is recognized as the induced-emf formulation for the mutual impedance Z_{on} between two sinusoidal dipoles. One of the dipoles has terminal current I_o and generates the field $\bar{E}^i$. The other is a center-fed linear dipole located on the z axis, centered at z_n, with unit terminal current and half-length s. Closed-form expressions and computer subroutines are available (12,13) for the mutual impedance Z_{on}.

Suppose we have used Equations (19) and (20) to calculate the current distribution I(z) at all the sampling stations $z = z_n$. Then it is a simple matter to determine the terminal impedance of the sinusoidal dipole in the presence of the wire as follows:

$$Z = Z_{oo} + (1/I_o) \sum_1^N I_n Z_{on} \tag{21}$$

where Z_{oo} denotes the terminal impedance of the dipole in free space.

F. Numerical Results and Summary

Figure 4 illustrates the admittance versus length for a center-fed antenna with radius "a" equal to the skin depth " δ ". The admittance was calculated with two independent techniques, and it may be noted that the results show excellent agreement. In the first technique, the traveling-wave theory given by Equations (5-9), the function $Y_1(z)$ was obtained with subroutine YFIN as described in Reference (10). The second technique is the sinusoidal-Galerkin moment method (13) with the surface-impedance formulation. Excellent agreement has also been observed for antennas with higher conductivity (a/δ= 2, 4, 8, 16 and ∞) and antennas with larger radius ($a = \ell/400$ with ℓ/λ ranging from 0.1 to 2.0). The agreement deteriorates, however, when the radius is less than the skin depth.

Figure 5 illustrates the backscatter echo-area patterns for straight wires with a/λ=1 and 4. Again the traveling-wave theory (Equations (10-14)) shows excellent agreement with the moment method (which has already been shown to agree with measurements (1)).

Figure 6 illustrates the current distribution induced on a straight wire by a nearby sinusoidal dipole. The Green's-function technique (Equations (16-20) shows excellent agreement with the moment method. Similar quality of agreement has been observed with parallel, perpendicular and coplanar-skew situations.

Figure 7 shows the broadside backscatter echo area of a perfectly conducting wire vs lengths up to 1.6, calculated using the piecewise sinusoidal Galerkin method (sufficiently segmented so that this solution is precise) and using the traveling-wave theory presented here. On the same figure appear comparable curves of the tumble receiver polarizations. This tumble average is calculated assuming equal likelihood for all possible aspects of the wire, and if a cloud of N of such chaff elements can be considered to be uncoupled, the cloud backscatter would be N times the tumble average value of the single element. The tumble average curve is seen to peak at $\ell/\lambda \approx 1$ while the broadside backscatter does not. This is due to the fact that upon tumbling, at off-broadside aspects, the odd current mode (appearing somewhat as a full sine wave) is excited and is strongly resonant, thereby contributing to average backscatter. By contrast, this mode is not excited when the wire is in broadside aspect due to its odd functional nature and so no resonant behavior is observed in the broadside backscatter curve in the vicinity of $\ell/\lambda = 1$.

Chaff is not perfectly conducting. Therefore Figure 8 shows the broadside backscatter and tumble average backscatter curves of practical aluminum-coated fiberlass chaff elements compared with those for the perfectly conducting case. We see very little difference between the two except in the resonance region around $\ell=n\lambda/2$. Figure 9 shows the curves of Figure 8 continued up to the region $6 < \ell/\lambda < 7$, and again, differences between perfectly conducting aluminum-coated fiberglass chaff are insignificant, except in the regions of resonance where about 1 dB less in tumble average echo appears. The data in Figures 7-9 also agrees quite well with other published data (14-15).

Three other approximate techniques were investigated for near-zone scattering problem involving a straight wire:

1. stationary phase

2. transmission-line model with $Y_i(z) \approx Y_o e^{-\gamma|z|}$

3. plane-wave approximation.

The "plane-wave approximation" refers to a simple generalization of Equations (10-14). All of these methods gave good results when the dipole was at least a distance of $\lambda/2$ away from the wire, but only the Green's-function technique maintains high accuracy when the distance is as small as $\lambda/10$.

In summary this work extends the traveling-wave theory to wires with finite conductivity, and presents a Green's-function technique for near-zone scattering by a straight wire.

G. Applications to Chaff Analysis

The traveling-wave theory has immediate application to plane-wave scattering by a "rope" element which may be many wavelengths in extent. It can be applied to an array of rope elements only if they are sufficiently far apart to permit an iterative solution. In its present form, the theory does not handle curved elements.

It is convenient to define a chaff element as "short" if the length is less than 0.6λ and "long" if the length exceeds 0.6λ. For a chaff cloud consisting of N short elements, one must solve an N x N matrix equation. Now if one adds a single long element to the cloud, the Green's-function technique allows one to solve the problem without increasing the size of the matrix. The addition of the long wire will change all the numbers in the N x N impedance matrix, but the new impedances are readily calculated. Instead of the free-space Green's-function, one now uses the Green's-function for the long wire.

For a chaff cloud containing N short elements and M long elements, the new technique is applicable only if the long elements are sufficiently far apart to permit an iterative solution.

We have not developed a model which takes into account coupling between two or more long elements in a chaff cloud, and at present it is not clear that the travelling wave model would remain valid for a long wire coupled to nearby long elements. In addition, the model applies only to straight long wires. If they are bent, as is likely to be the case with a physically long slender chaff element, the travelling wave model is not valid in its present form.

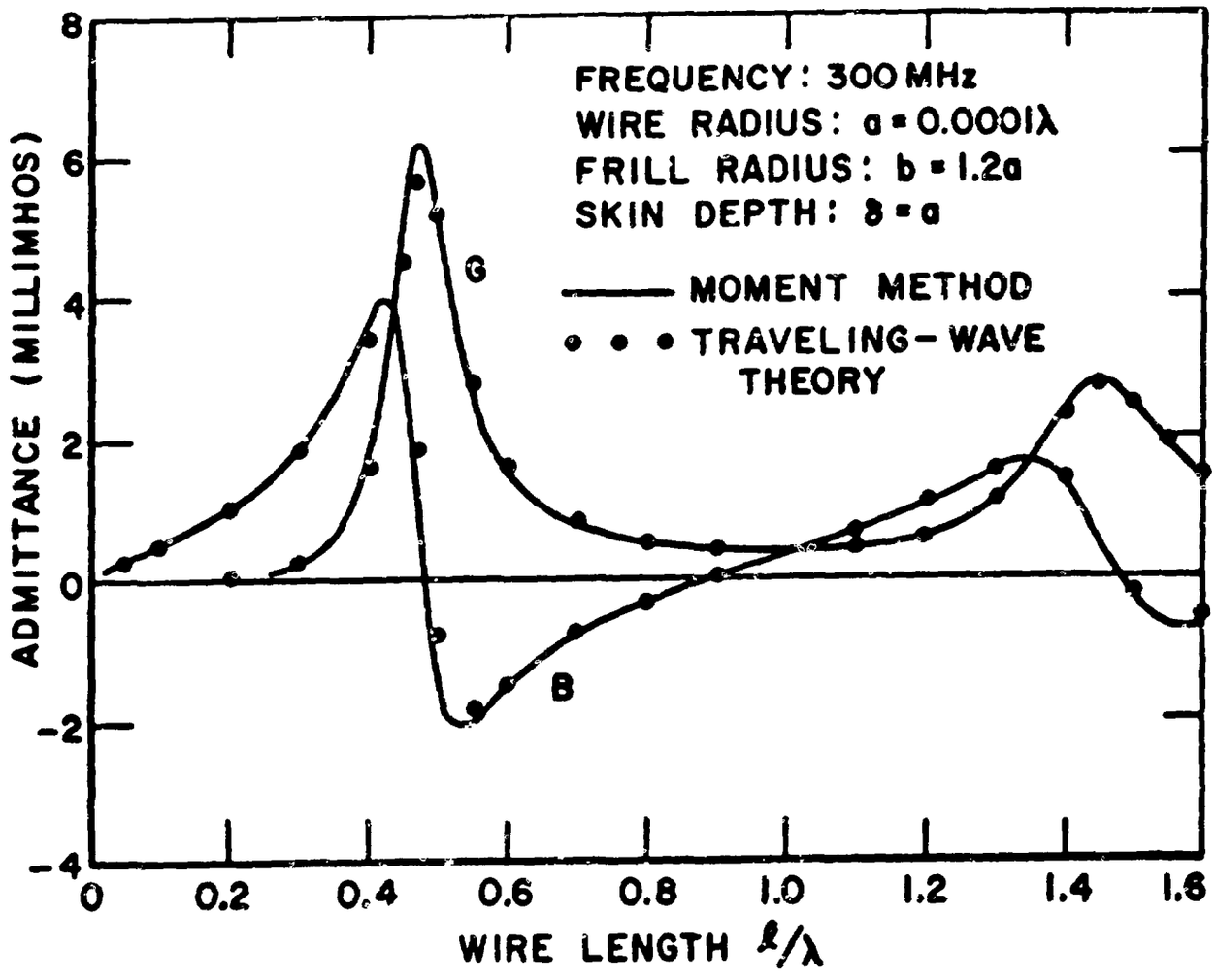

Figure 4. Admittance Versus Length for Imperfectly-conducting Center-fed Cylindrical-wire Antenna.

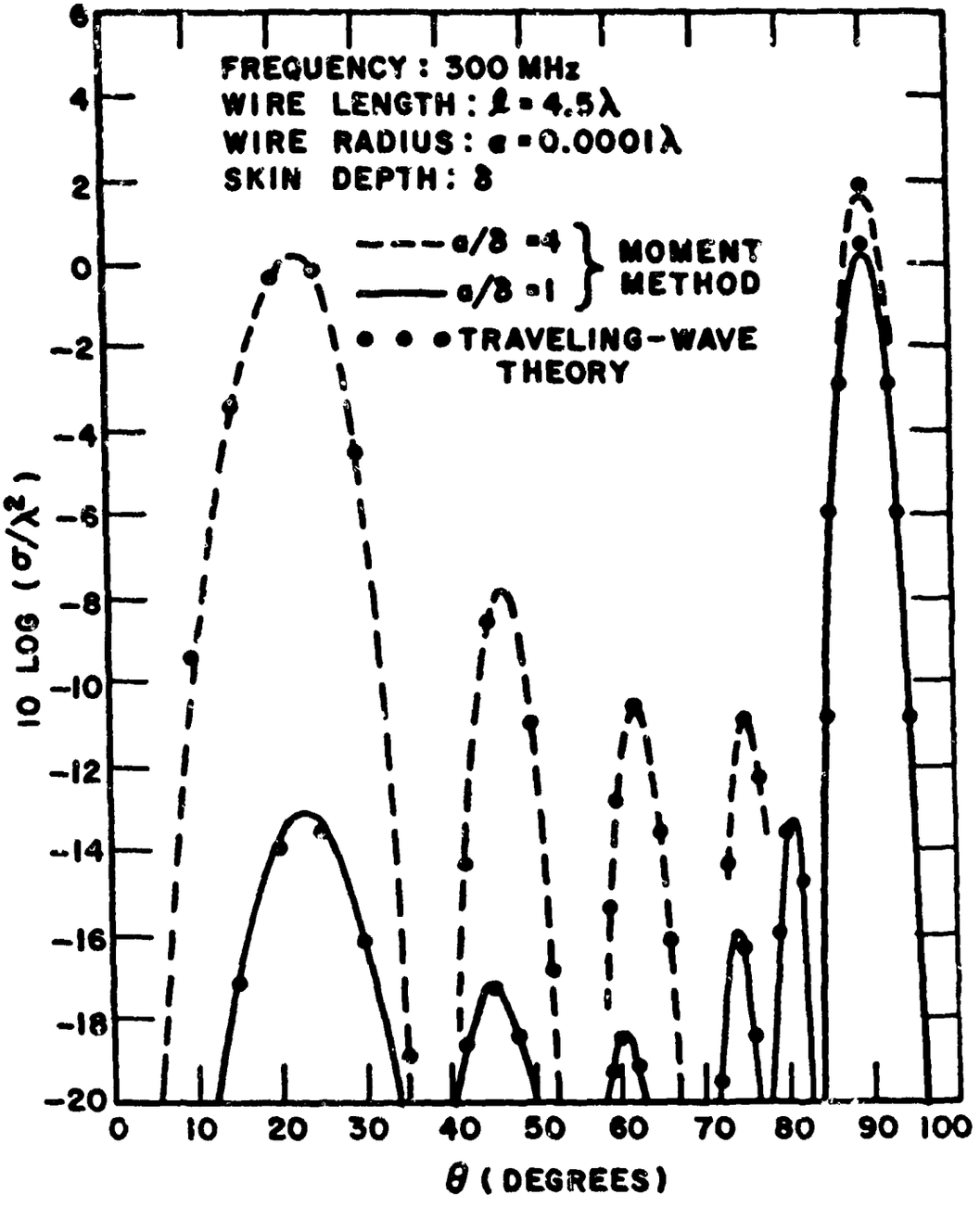

Figure 5. Backscatter Echo Area Versus Aspect for Imperfectly-conducting Straight Wire.

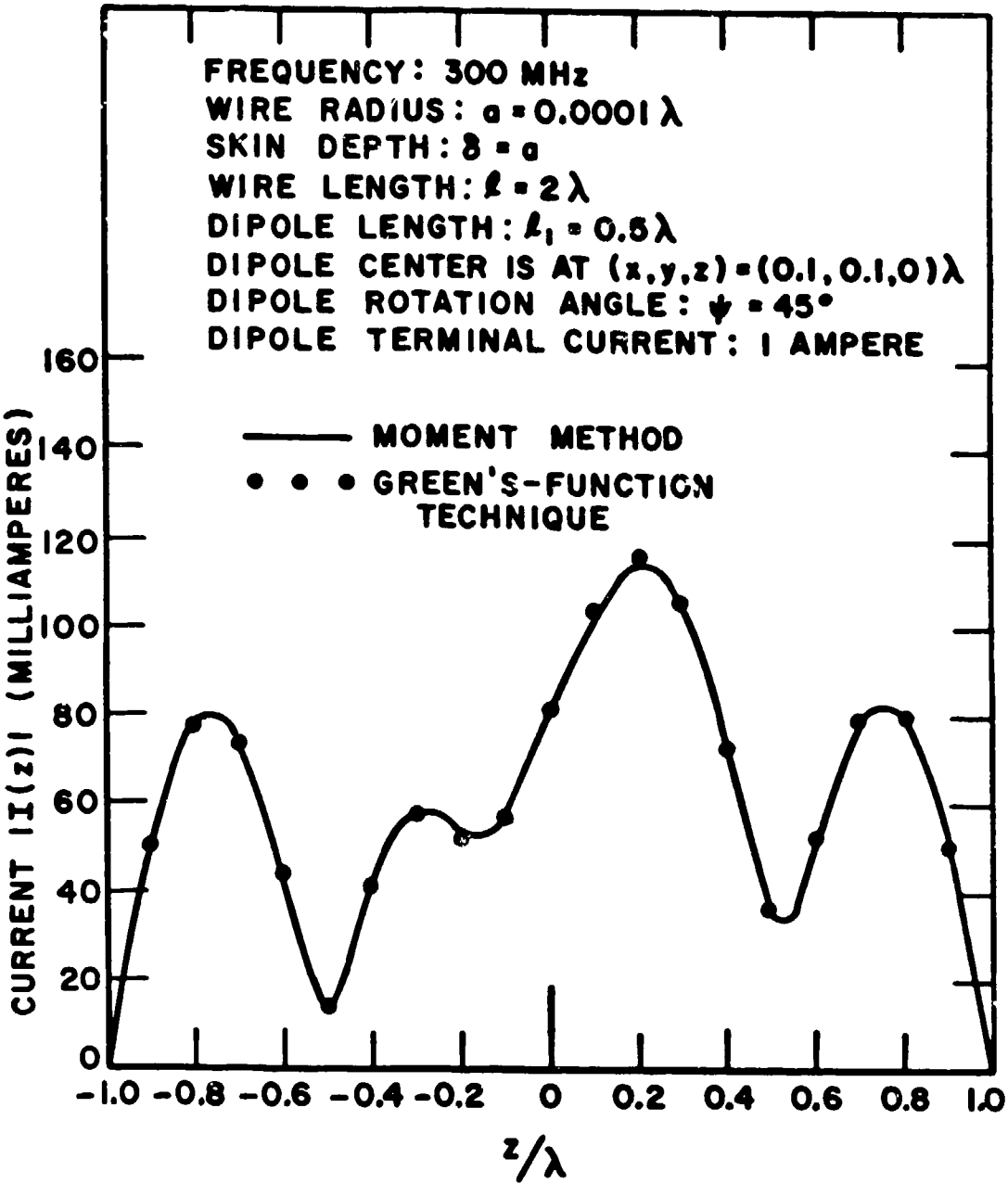

Figure 6. Current Distribution Induced on Thin Wire by Nearby Center-fed Sinusoidal Dipole, with Nonplanar Skew Situation.

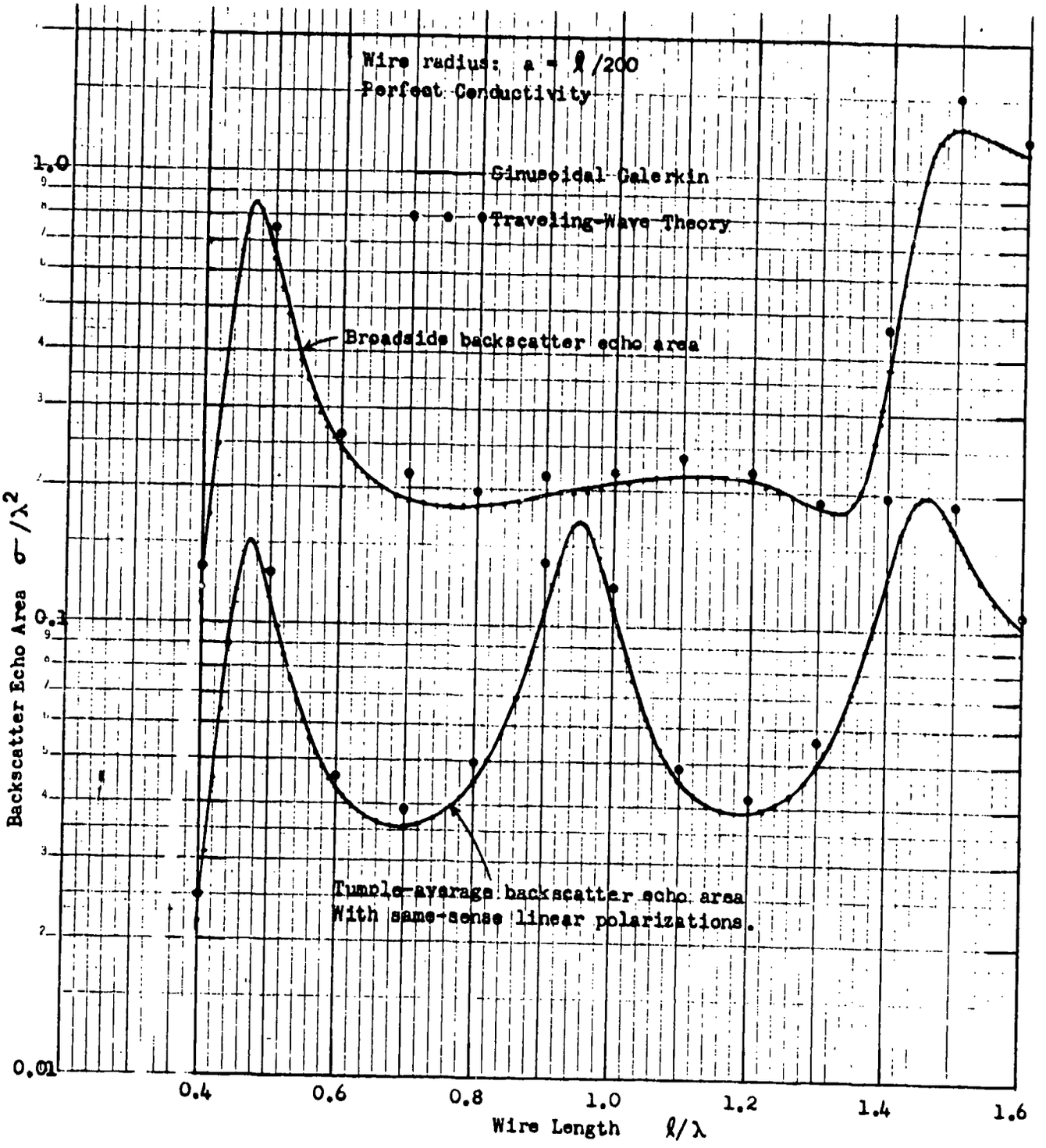

Figure 7. Broadside and Tumble Average Echo Areas of a Perfectly Conducting Wire Element Using "Exact" Sinusoidal Galerkin Method and Approximate Travelling Wave Theory.

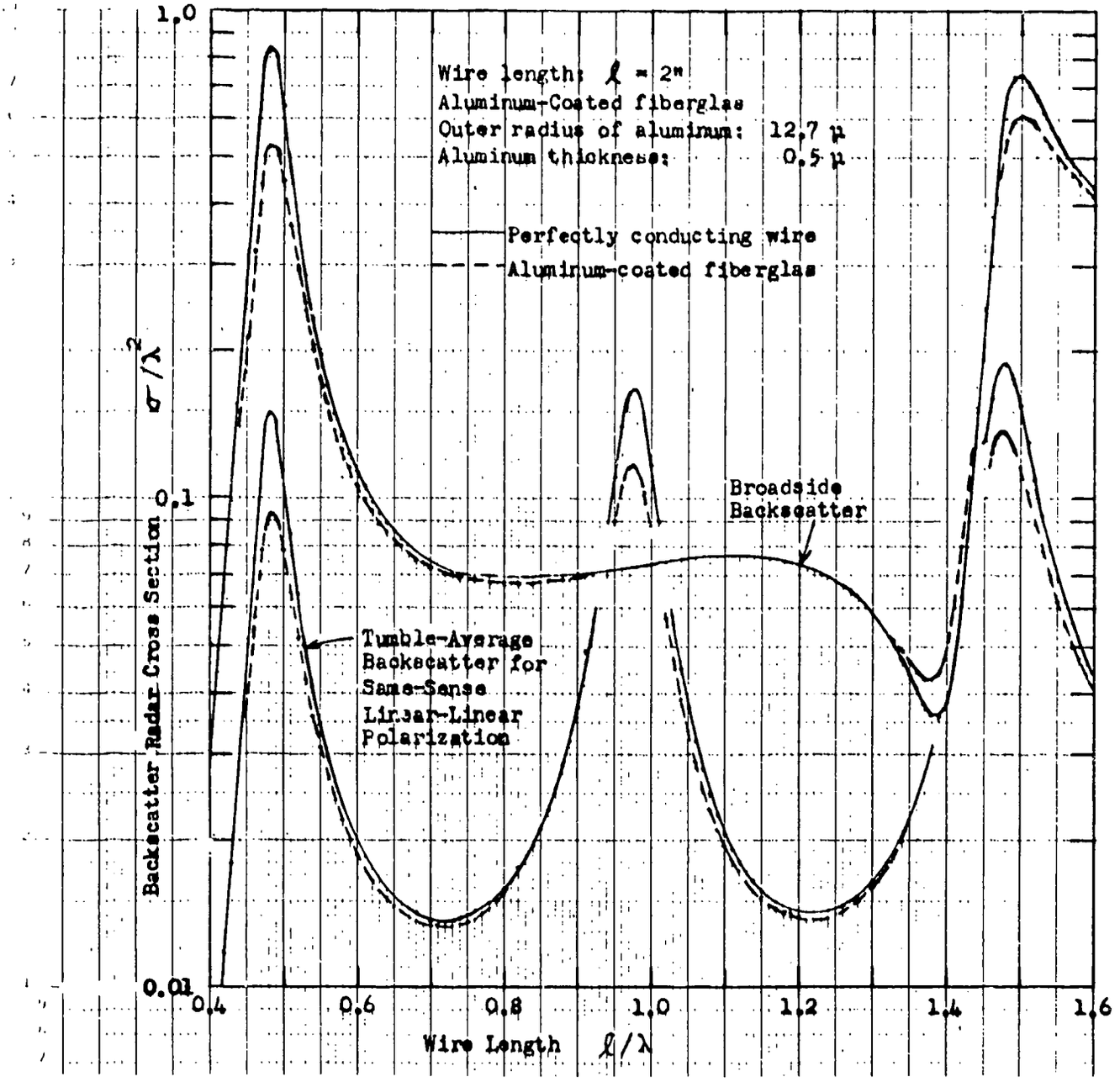

Figure 8. Comparison of the Broadside and Tumble Average Echo Areas of Perfectly Conducting and Aluminum-coated Fiberglass Chaff Elements.

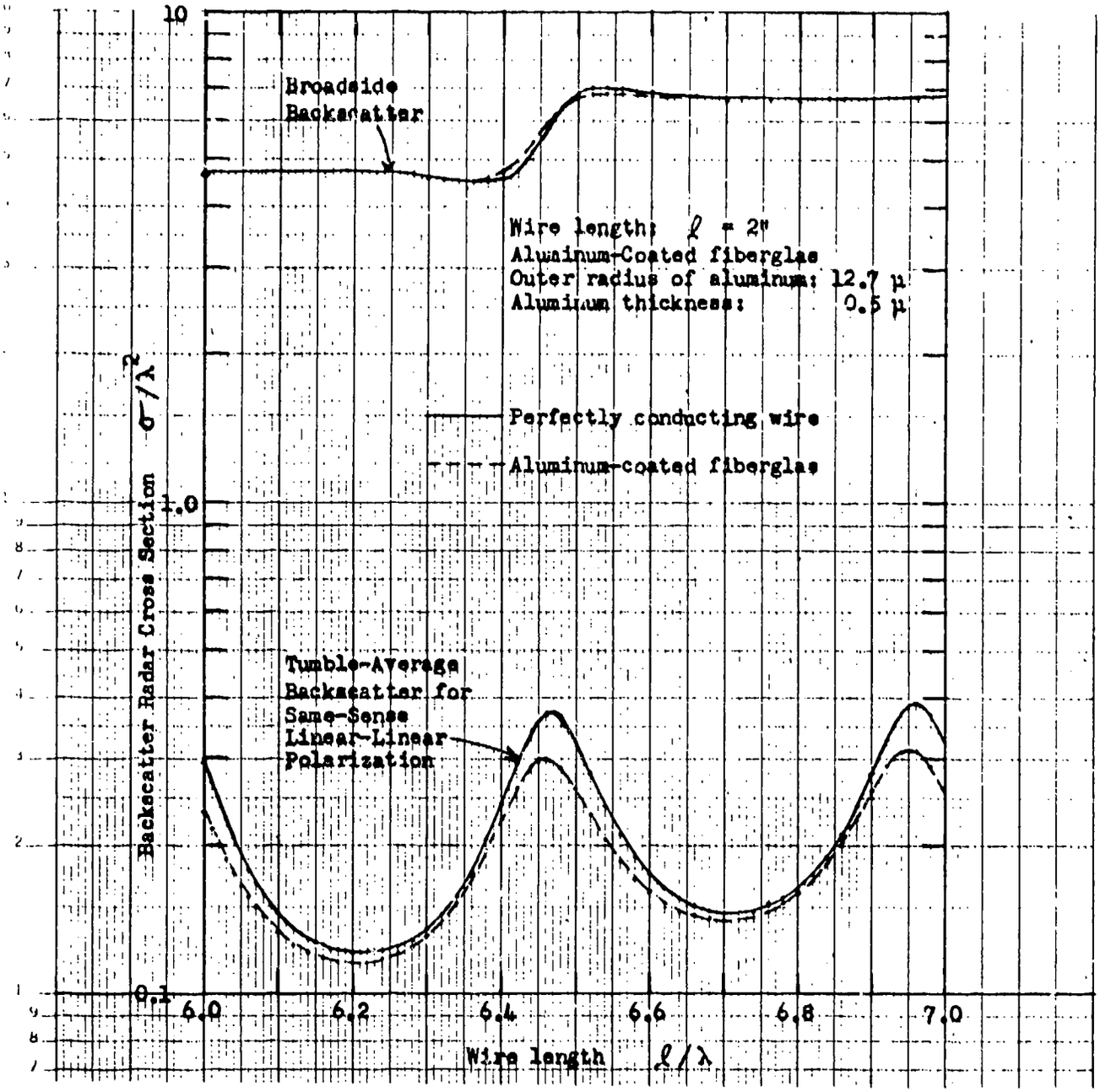

Figure 9. Continuation of the Curves of Figure 8 into the Region $6 \leq \ell/\lambda \leq 7$.

SECTION III
MEASUREMENTS OF SOME CHAFF-COATED FOAM

A. Circular Disks

In an effort to observe the backscatter characteristics of ensembles of extremely dense chaff dipoles, measurements were made of the backscattering cross section of foam disks coated with aluminum strip chaff which were cut to be resonant at 10 GHz. Figures 10 and 11 are photographs of the two 8" diameter disks. The dipoles were adhered to the disks and to each other by a spray adhesive and were sprinkled on in several layers to a thickness of about 2 cm. The finished surface appeared almost like silvered grass. Uniform density of dipoles across each disk was achieved by back-lighting the disks and observing the percentage of shadowing created by the deposit of dipoles. No strict numerical measure of the dipole density was attempted.

Backscattering patterns at 10 GHz were recorded for same-sense and crossed-linear polarizations for look-angles $\pm 90^{\circ}$ from broadside. Eighteen pairs of such patterns were recorded for each disk - one pair for each 10° rotation of the circular panel around the line-of-sight axis (i.e., the panel normal). Typical patterns are shown in Figures 12 and 13, one each for same-sense and crossed-sense polarizations. Each such pattern was stored in a computer memory (every 1° of rotation), and the scattered power averaged over a window which was $\pm 7\frac{1}{2}^{\circ}$ wide, centered about the look angle. The resulting 18 smoothed curves were stored and then these were averaged together look-angle by look-angle. The resulting smoothed and averaged curves are those shown in Figures 14 and 15 for the two separate plates shown in Figures 10 and 11. The broadside-specular reflection from an 8" circular flat metallic plate is shown for reference on all the figures.

The difference between the same-sense and crossed returns consistently appears to be about 5 dB for look-angles away from normal incidence; near normal incidence, the difference rises to about 13 dB. This suggests that it might be useful to decompose the return into a randomly polarized component and a spherelike component and observe the change in ratios of the two components as the obstacle is viewed from broadside to far-off broadside. Such an analysis follows.

At a single aspect and source frequency, the polarization properties of reflections from an object are described by a 2x2 symmetric matrix with complex elements. For a target such as the dense wire ensembles formed by the chaff coated disks, the elements of this matrix would vary erratically in amplitude and phase, as a function of aspect. However, the averaged polarization properties for a target can be described by a 4x4 real symmetric matrix which predicts the average power received as a function of transmit-receive polarizations over any specified range of aspects (or frequencies) (16). If all aspects about the line of sight differing only by a rotation about the line of sight are equally likely and if the target has no sense preference; i.e., equal average power and returns for right-to-right and left-to-left circular transmit-receive polarizations may be expected, the average scattering matrix reduces to diagonal form, where

Figure 10. Photograph of 8" Foam Disk Coated with Aluminum Strip Chaff.

Figure 11. Photograph of 8" Foam Disk Coated with Aluminum Strip Chaff.

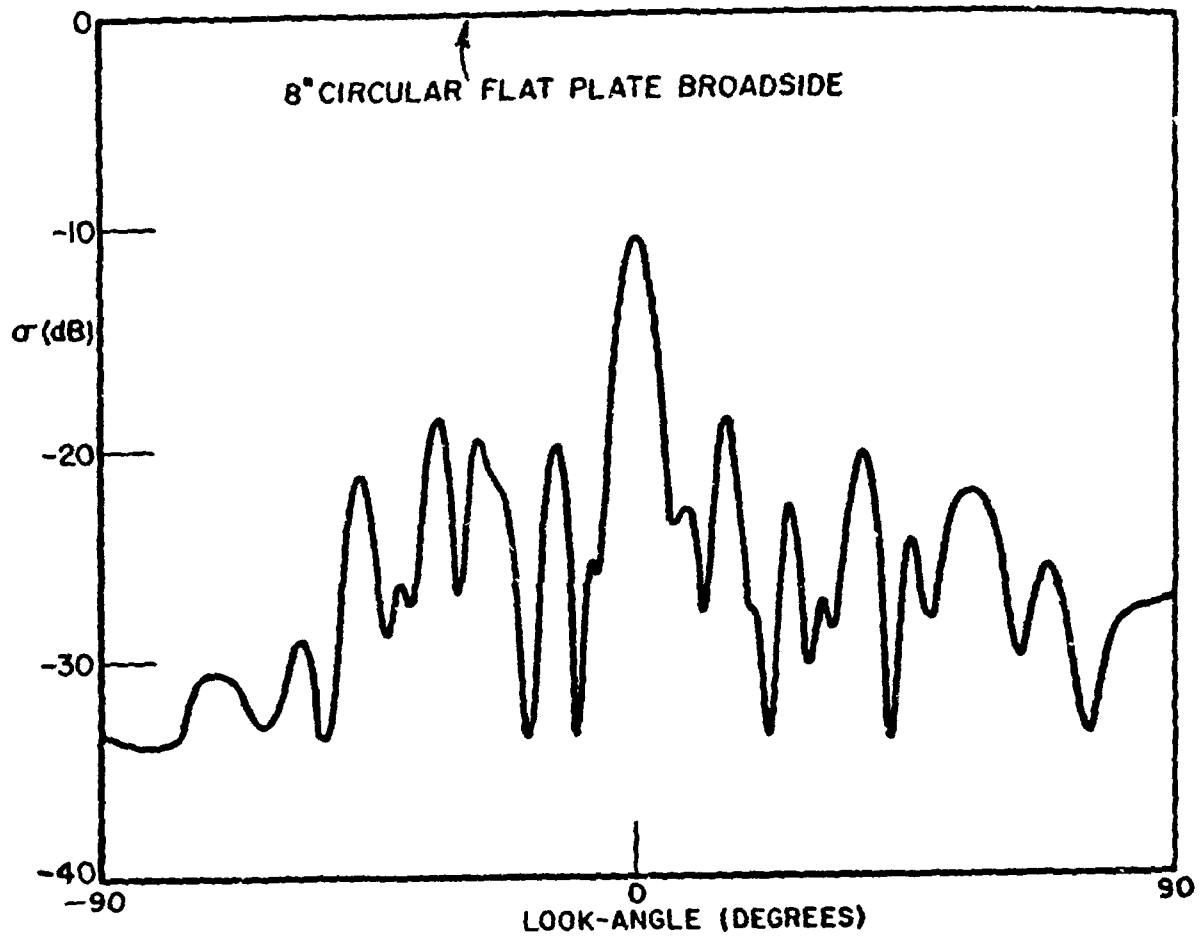

Figure 12. A Typical Backscattering Pattern from the Disks of Figures 10 and 11. Horizontal-to-horizontal Polarization.

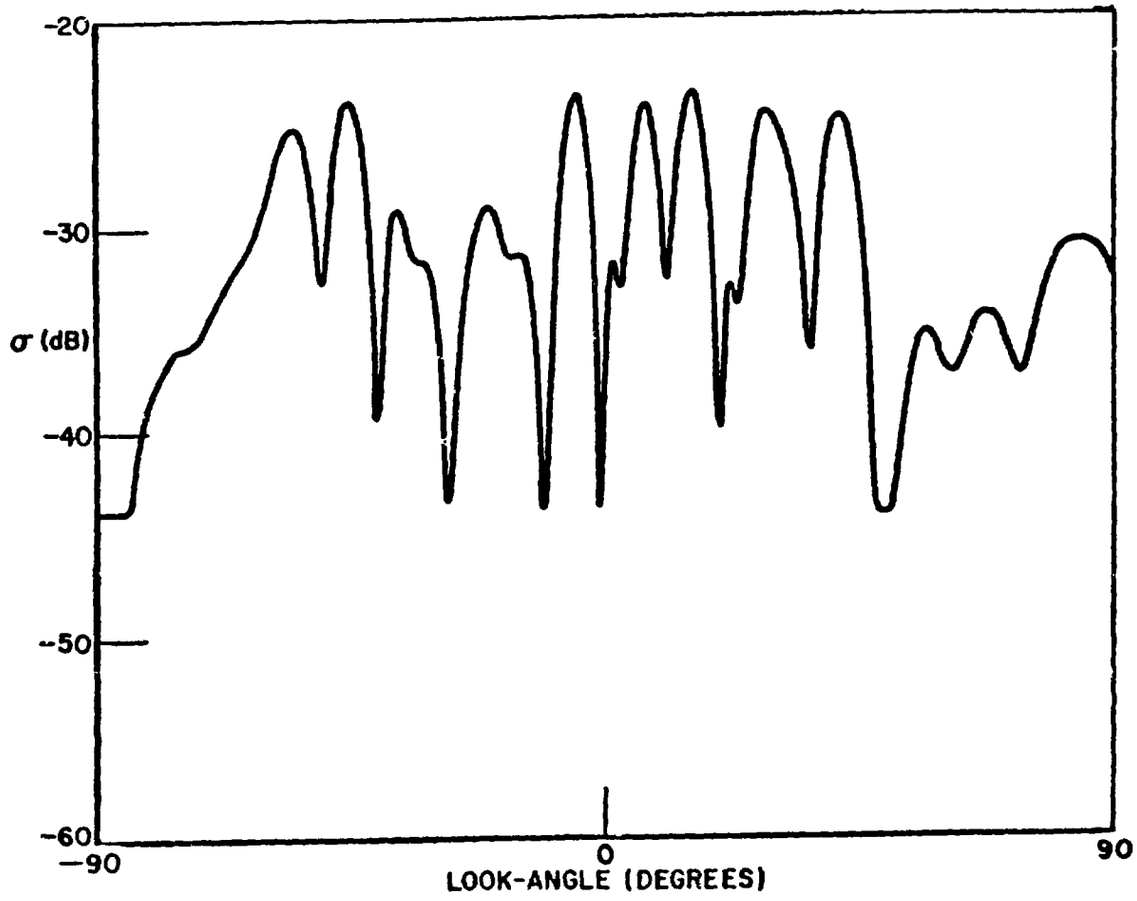

Figure 13. A Typical Backscattering Pattern from the Disks of Figures 10 and 11. Horizontal-to-vertical Polarization.

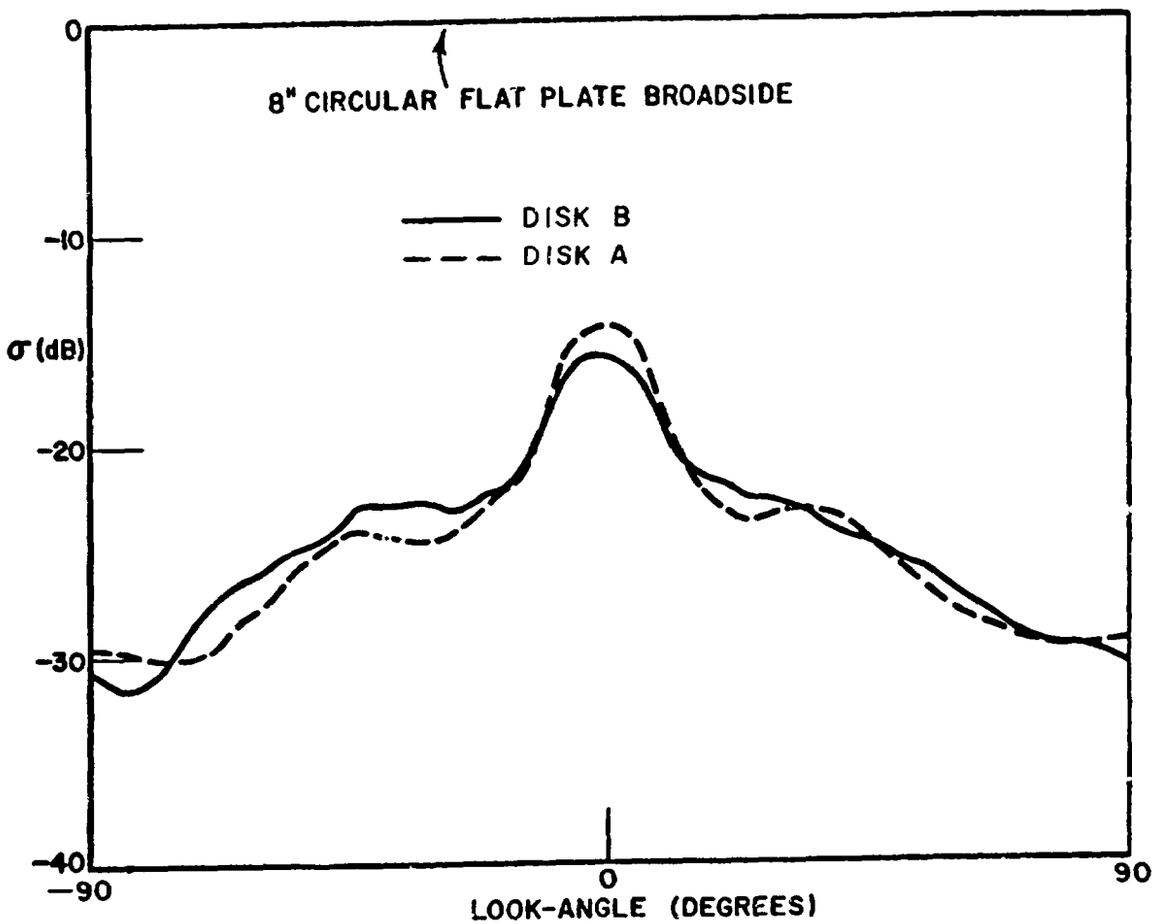

Figure 14. Smoothed and Averaged Backscatter of Two 8" Diameter Chaff Disks Versus Look Angle from Broadside at f = 10 GHz. Horizontal-to-horizontal Polarization.

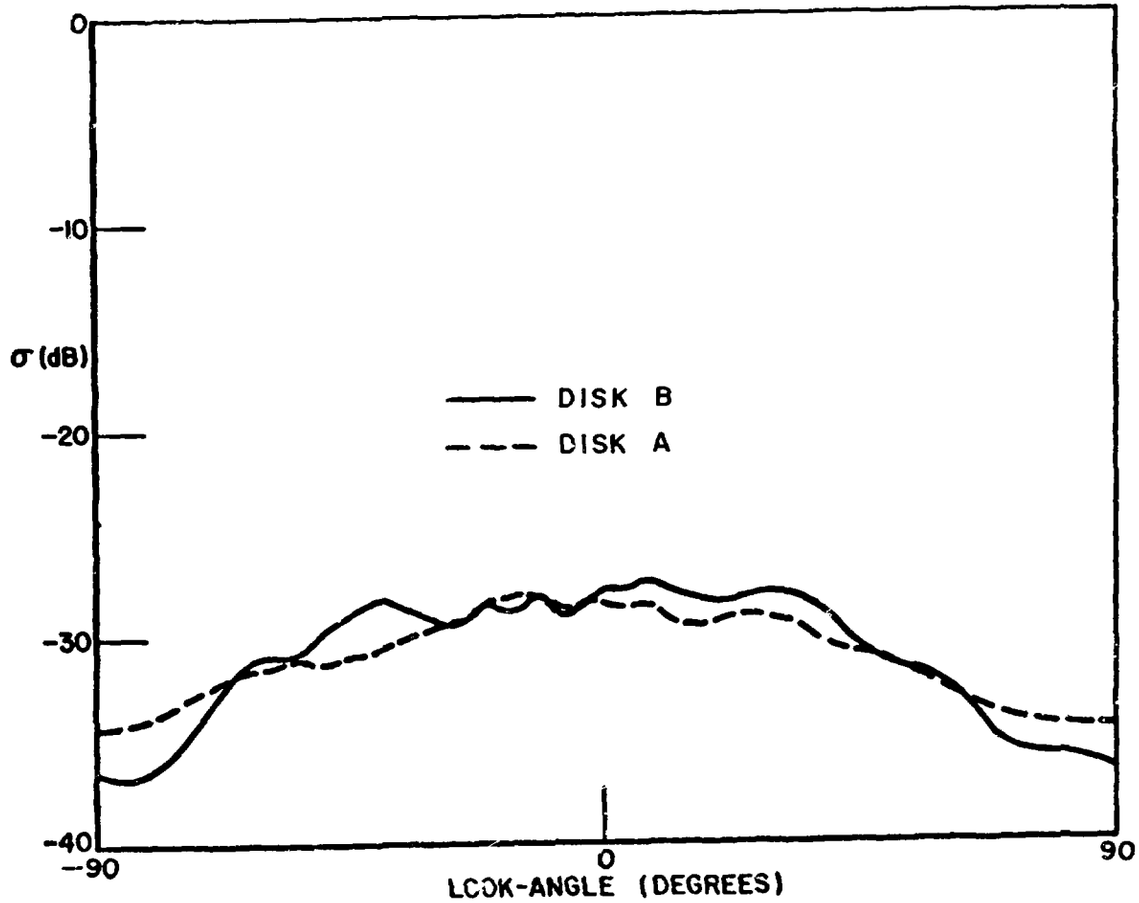

Figure 15. Averaged Backscatter of Two 8" Diameter Chaff Disks Versus Look Angle from Broadside at f = 10 GHz. Horizontal-to-vertical Polarization.

$$(S_{av}) = \begin{pmatrix} \lambda_1 & 0 & 0 & 0 \\ 0 & \lambda_2 & 0 & 0 \\ 0 & 0 & \lambda_3 & 0 \\ 0 & 0 & 0 & \lambda_4 \end{pmatrix} \tag{22}$$

and where $\lambda_1 = \lambda_2 + \lambda_3 + \lambda_4$ and $\lambda_2 = \lambda_3$ (17). To obtain the average power returned from the target with a given choice of transmit receive polarizations, the matrix (S_{av}) is multiplied on the right by a 4-element column vector P_T corresponding to the transmit polarization, and on the left by a 4-element row vector P_R corresponding to the receive polarization where

$$P_T = \begin{pmatrix} 1 \\ X_T \\ Y_T \\ Z_T \end{pmatrix} \qquad P_R = (1\ X_R\ Y_R\ Z_R); \tag{23}$$

and where the components X,Y,Z are the rectangular coordinates of the point on the polarization sphere of unit radius denoting the antenna polarization (17). Thus, for vertical linear polarization

$$P_T = \begin{pmatrix} 1 \\ 1 \\ 0 \\ 0 \end{pmatrix} \qquad P_R = (1\ 1\ 0\ 0); \tag{24}$$

for horizontal linear polarization

$$P_T = \begin{pmatrix} 1 \\ -1 \\ 0 \\ 0 \end{pmatrix} \qquad P_R = (1\ -1\ 0\ 0); \tag{25}$$

for right circular polarization

$$P_T = \begin{pmatrix} 1 \\ 0 \\ 0 \\ 1 \end{pmatrix} \qquad P_R = (1\ 0\ 0\ 1); \tag{26}$$

for left circular polarization

$$P_T = \begin{pmatrix} 1 \\ 0 \\ 0 \\ -1 \end{pmatrix} \qquad P_R = (1\ 0\ 0\ -1). \tag{}$$

As indicated previously, to describe the average polarization properties of the dense chaff disks, the received power was averaged over 15^0 azimuth angle variations as the ensemble was rotated about an axis perpendicular to the line of sight and corresponding 15^0 averages were averaged for 18 different cuts obtained by rotating the entire ensemble about the line of sight (at broadside) in 10^0 increments. Measurements of the average power received for horizontal-horizontal and horizontal-vertical transmit-receive polarizations were made. Thus for the matrix (S_{av}) of the form assumed

Horizontal-Horizontal - Average Power W_{HH}

$$W_{HH} = (1\ -1\ 0\ 0)\begin{pmatrix} \lambda_1 & 0 & 0 & 0 \\ 0 & \lambda_2 & 0 & 0 \\ 0 & 0 & \lambda_3 & 0 \\ 0 & 0 & 0 & \lambda_4 \end{pmatrix}\begin{pmatrix} 1 \\ -1 \\ 0 \\ 0 \end{pmatrix} = \lambda_1 + \lambda_2 \tag{28}$$

Horizontal-Vertical - Average Power W_{HV}

$$W_{HV} = (1\ 1\ 0\ 0)\begin{pmatrix} \lambda_1 & 0 & 0 & 0 \\ 0 & \lambda_2 & 0 & 0 \\ 0 & 0 & \lambda_3 & 0 \\ 0 & 0 & 0 & \lambda_4 \end{pmatrix}\begin{pmatrix} 1 \\ -1 \\ 0 \\ 0 \end{pmatrix} = \lambda_1 - \lambda_2 \tag{29}$$

$$\lambda_1 = \frac{1}{2}\ (W_{HH} + W_{HV}) \tag{30a}$$

$$\lambda_2 = \frac{1}{2}\ (W_{HH} - W_{HV}) = \lambda_3 \tag{30b}$$

$$\lambda_4 = \lambda_1 - 2\lambda_2 = \frac{1}{2}\ (3W_{HV} - W_{HH}) \tag{30c}$$

Thus, from the measured data, it is possible to compute the diagonal elements of the average scattering matrix of the dense chaff ensemble, at any 15^{o} azimuth sector a specified angular distance up to 45^{o} from the normal. The averaged power returns are those shown in Figures 14 and 15, where the results for two different plates have been presented to give an idea of the variation between samples. A general maximum is obtained in the horizontal-horizontal return at broadside to the plane of the wire ensemble, and at the peak W_{HH} is approximately 13 dB higher than W_{HV}. For other aspects, W_{HH} is roughly 5 dB higher than W_{HV}. The elements of the average scattering matrix can be obtained from these data and some general conclusions may be drawn from the trends observed.

It is possible to consider (S_{av}) as the incoherent superposition of a randomly polarized component with $\lambda_2^r = \lambda_3^r = \lambda_4^r = 1/3\ \lambda_1^r$, and a sphere-like component with $\lambda_2^s = \lambda_3^s = -\lambda_4^s = \lambda_1^s$. Then, a little algebra shows that the ratio of the sphere-like component λ_1^s to the random component λ_1^r is given by

$$\frac{\lambda_1^s}{\lambda_1^r} = \frac{W_{HH}}{3W_{HH}} - 2/3. \tag{31}$$

At broadside, where W_{HH} is 13 dB above W_{HV}, the ratio of the sphere-like component to the random is

$$\frac{\lambda_1^s}{\lambda_1^r} = 6 = 7.8 \text{ dB}. \tag{32}$$

At aspects outside of broadside, where W_{HH} is 5 dB above W_{HV},

$$\frac{\lambda_1^s}{\lambda_1^r} = 0.4 = -4.1 \text{ dB}. \tag{33}$$

Thus, for aspects other that the broadside region, we may say the dense ensemble of dipoles closely approximates a "random" target, for which the average return from any common transmit-receive polarization is the same, while the average return from any orthogonal transmit-receive polarization combination is down by 3 dB. The presence of a weak sphere-like component changes this ratio to 5 dB for linear polarization. For aspects close to broadside the sphere-like component increases to a level approximately 8 dB above that of the random component.

For aspects off broadside, we may compare the average scattering matrix of the chaff ensemble with that for a randomly oriented (about the line of sight) thin wire. For such a target, it may be shown that

$$(S_{av}) = \begin{pmatrix} \lambda_1 & 0 & 0 & 0 \\ 0 & \lambda_1/2 & 0 & 0 \\ 0 & 0 & \lambda_1/2 & 0 \\ 0 & 0 & 0 & 0 \end{pmatrix} \tag{34}$$

and the ratio of returns for horizontal-horizontal and horizontal-vertical transmit-receive polarization is

$$\frac{W_{HH}}{W_{HV}} = \frac{3/2\ \lambda_1}{1/2\ \lambda_1} = 3 = 4.8\ \text{dB}, \tag{35}$$

which agrees closely with that observed for the chaff ensemble off broadside. Thus, as far as polarization properties are concerned, it may be modelled by an ensemble of arbitrarily oriented thin wires.

B. A Simulated Dense Chaff Cloud

A series of backscattering measurements were made on a target which "simulated" a chaff cloud. The target consisted of a foam circular cylinder 9 3/4" in diameter capped at both ends by hemispheres of the same diameter, the entire unit being 70" long. This foam shape was coated with a random sprinkling of aluminum chaff elements (s through x band lengths) held in place by spray adhesive and layered to a thickness of about 1" as uniformly as could be gauged by the eye. The target was held aloft by skewers in each end nestled in a string support, and it was rotated with its longitudinal axis parallel to the floor at the same height as the viewing radar antenna. Radar backscattering (actually, 5° bistatic) patterns (horizontal-horizontal polarization) were recorded for 360° of rotation for each of six orientations of the cylinder about its own longitudinal axis - 0°, $\sim 30^\circ$, $\sim 60^\circ$, $\sim 90^\circ$, $\sim 120^\circ$, $\sim 150^\circ$. This gave six patterns (five at 14 GHz) each at four frequencies, 10 GHz, 12 GHz, 14 GHz and 16 GHz. The only regions of interest of these 360° patterns were those $\pm 10^\circ$ about the head and tail ends of the target. The incident wavefront could not be considered planar over an area any larger than the projected areas within these near-endfire limits, so the patterns beyond the endfire regions were considered to be of little value for the purposes at hand.

Every 360° pattern was referenced to the broadside backscatter from a 6 3/4" square flat plate and recorded in a computer file. Then each target pattern was smoothed by averaging the cross sections over a sliding window 6° wide. A typical 360° pattern and its smoothed version are shown in Figure 16 where 0° represents the head of the target and $\pm 180^\circ$ represents its tail. The 0 dB level is that of the reference plate in every case. Similar smoothed 360° patterns for each of the frequencies 10 GHz, 12 GHz, 14 GHz, and 16 GHz, respectively were recorded and averaged over each frequency group and then averaged over both the head and tail regions. The resulting smoothed and averaged patterns are shown in Figures 17-20 on an expanded scale elaborating the region $\pm 20^\circ$ from end-fire. Only the region $\pm 10^\circ$ should be considered valid in these patterns.

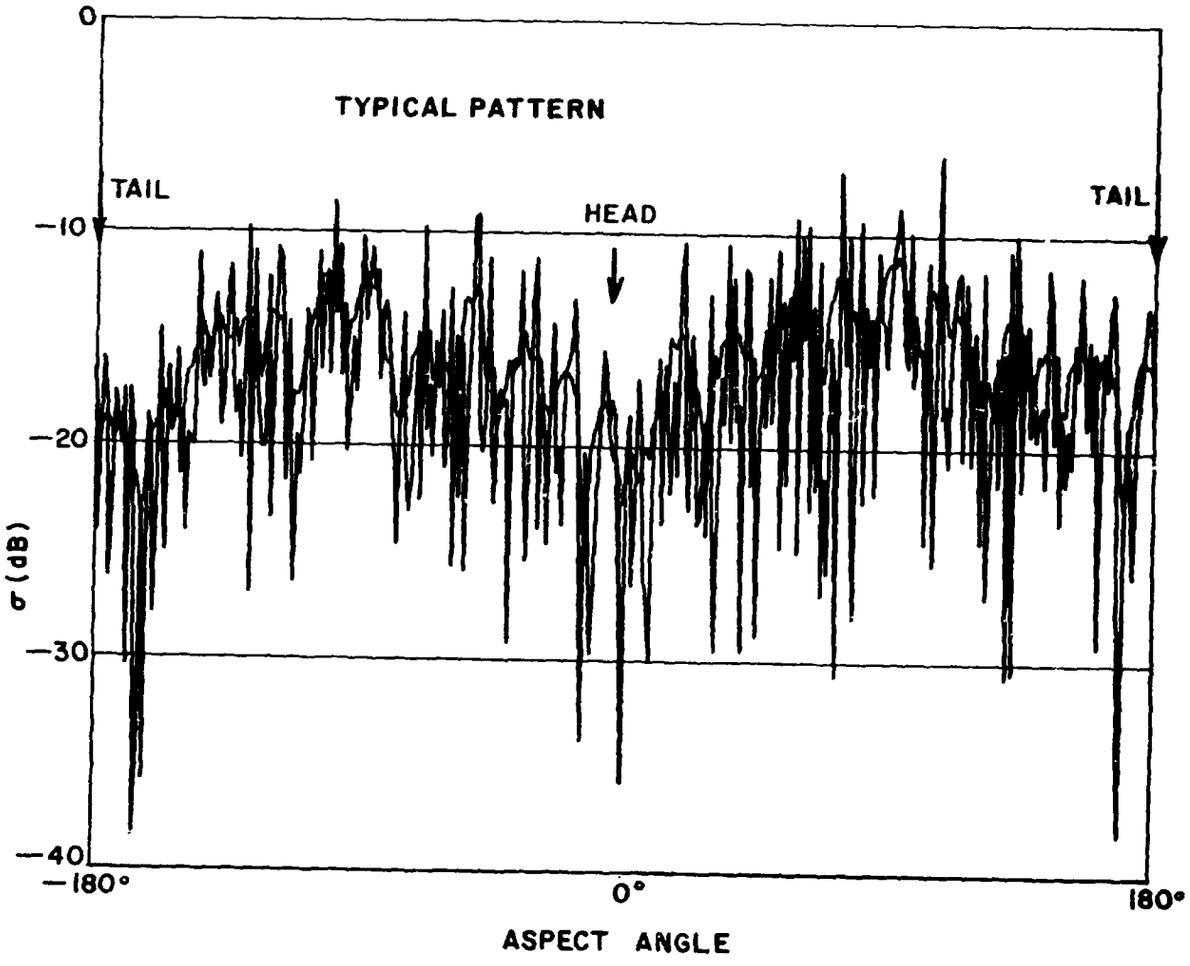

Figure 16. Typical Pattern of 70" Sphere Capped Cylinder (Chaff Cloud Model). Only the Head and Tail Regions are Considered Meaningful.

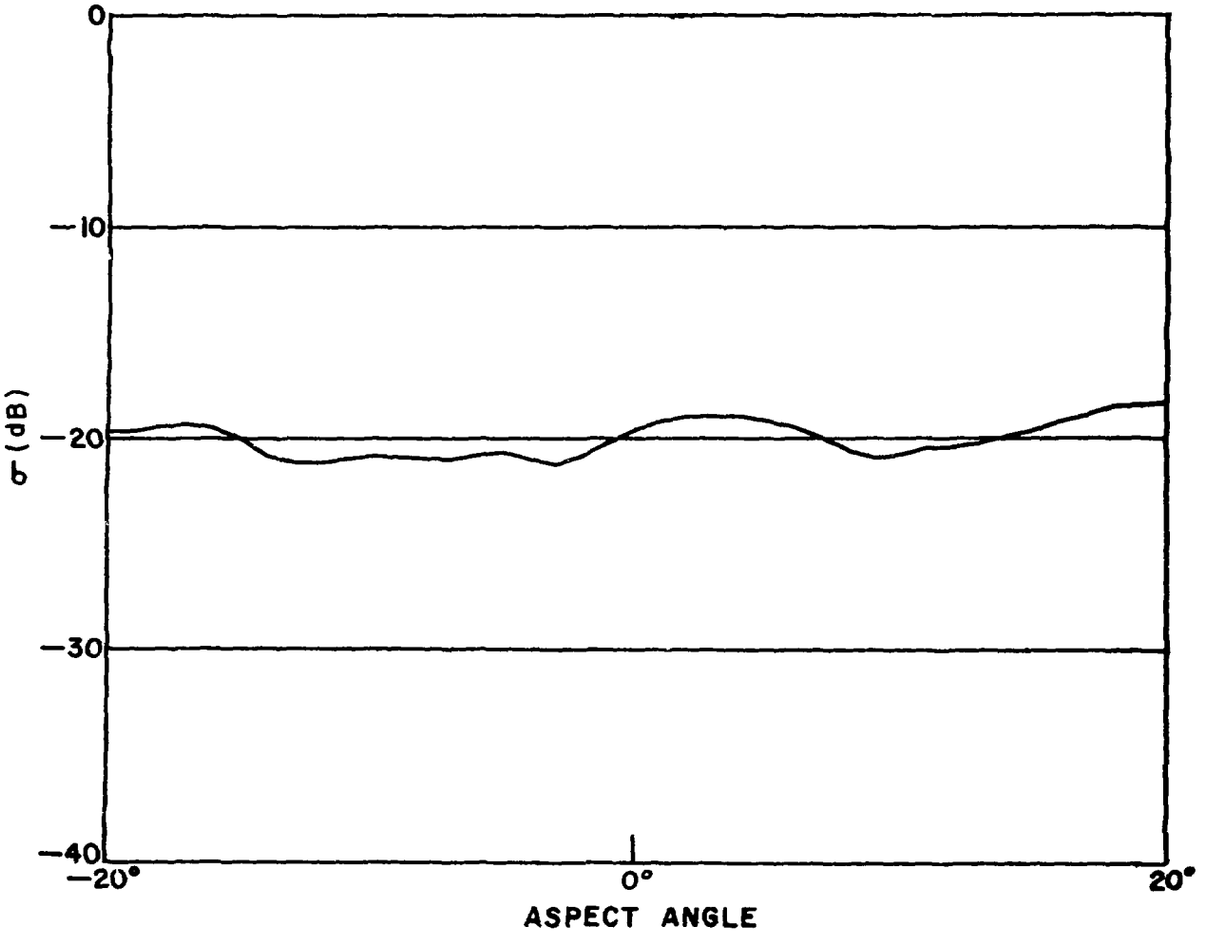

Figure 17. Smoothed and Averaged Backscatter from Nose and Tail Region of 70° Sphere-capped Cylinder (Chaff Cloud Model). f = 10 GHz.

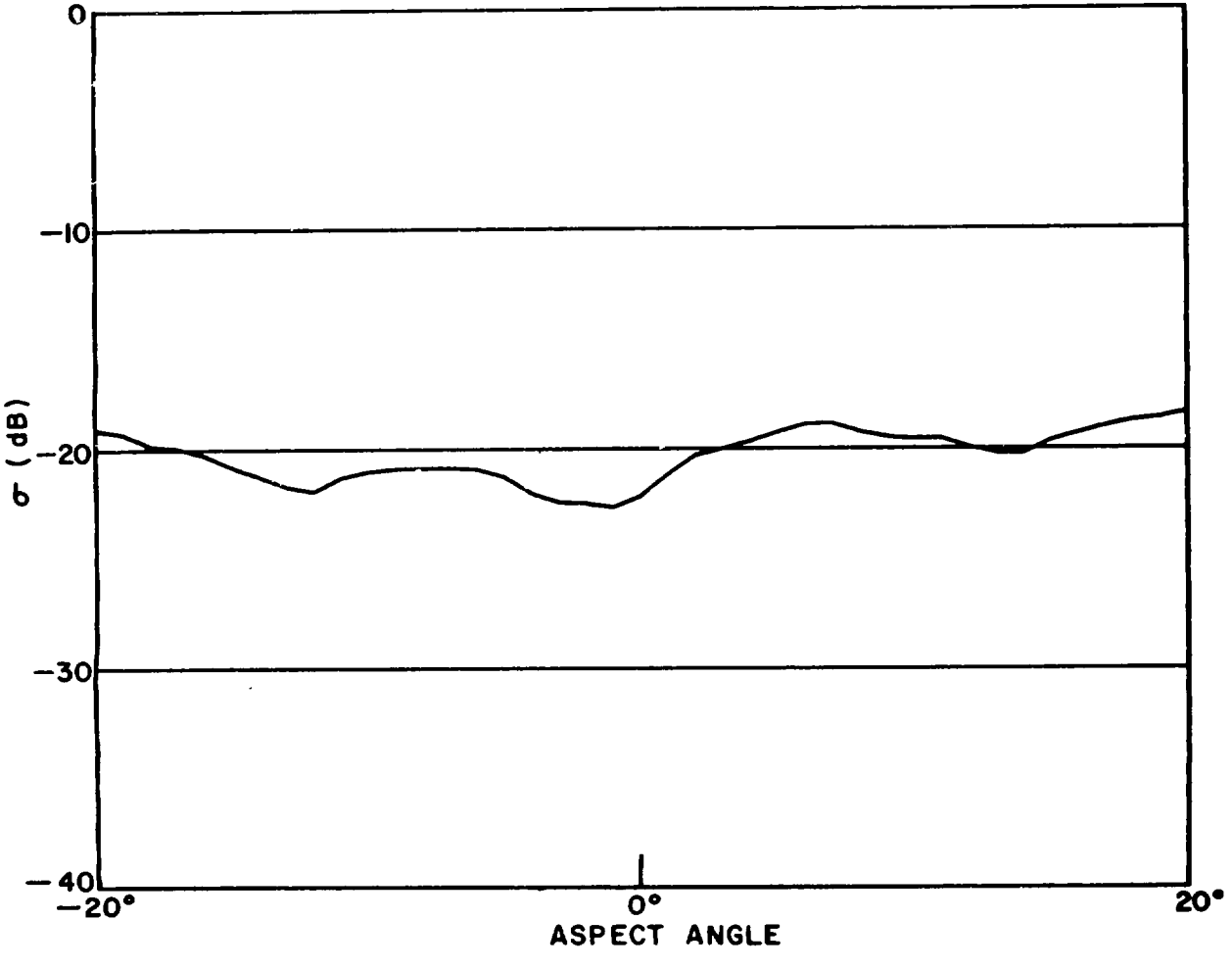

Figure 18. Smoothed and Averaged Backscatter from Nose and Tail Region of 70° Sphere-capped Cylinder (Chaff Cloud Model). f = 12 GHz.

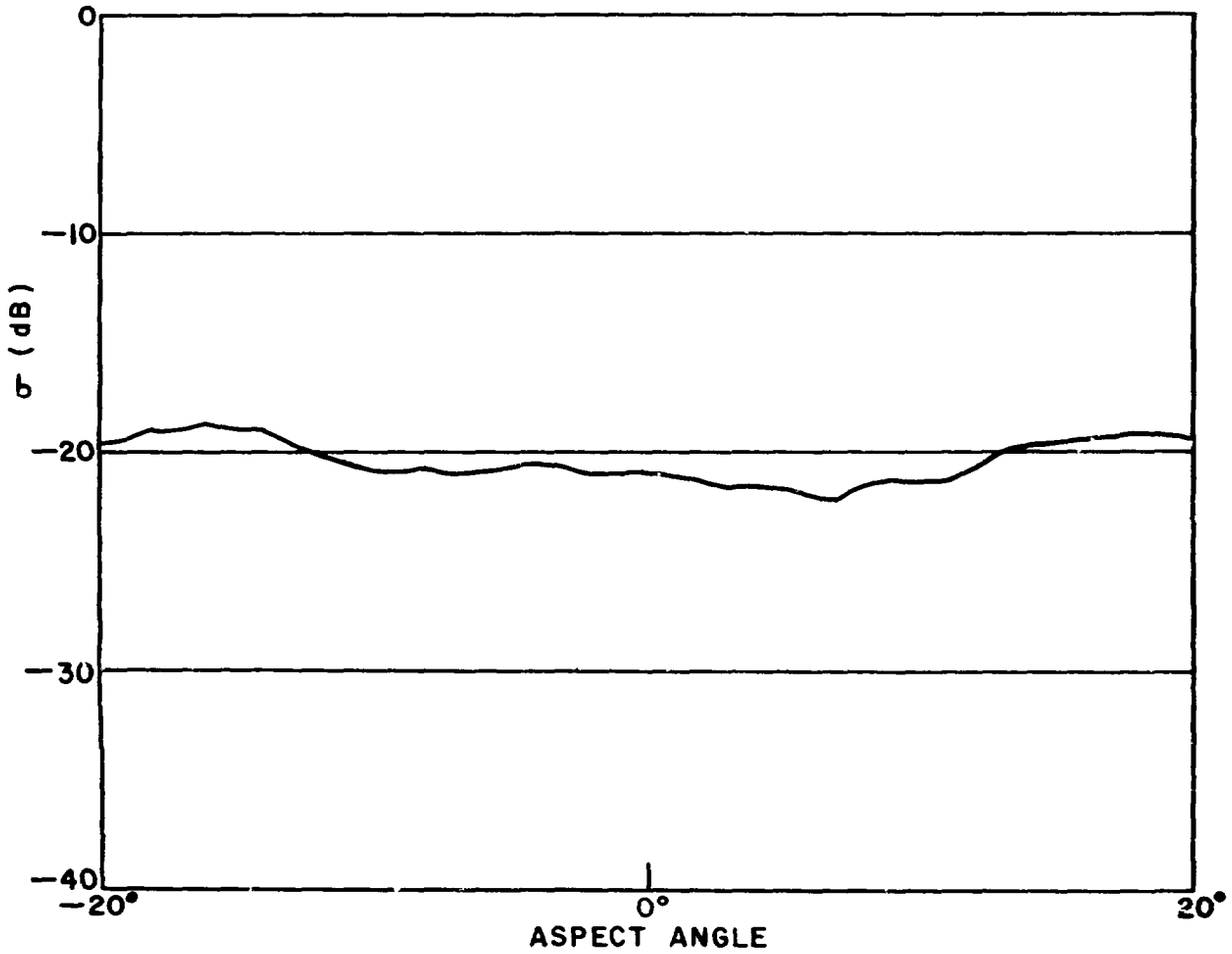

Figure 19. Smoothed and Averaged Backscatter from Nose and Tail Region of 70° Sphere-capped Cylinder (Chaff Cloud Model). f = 14 GHz.

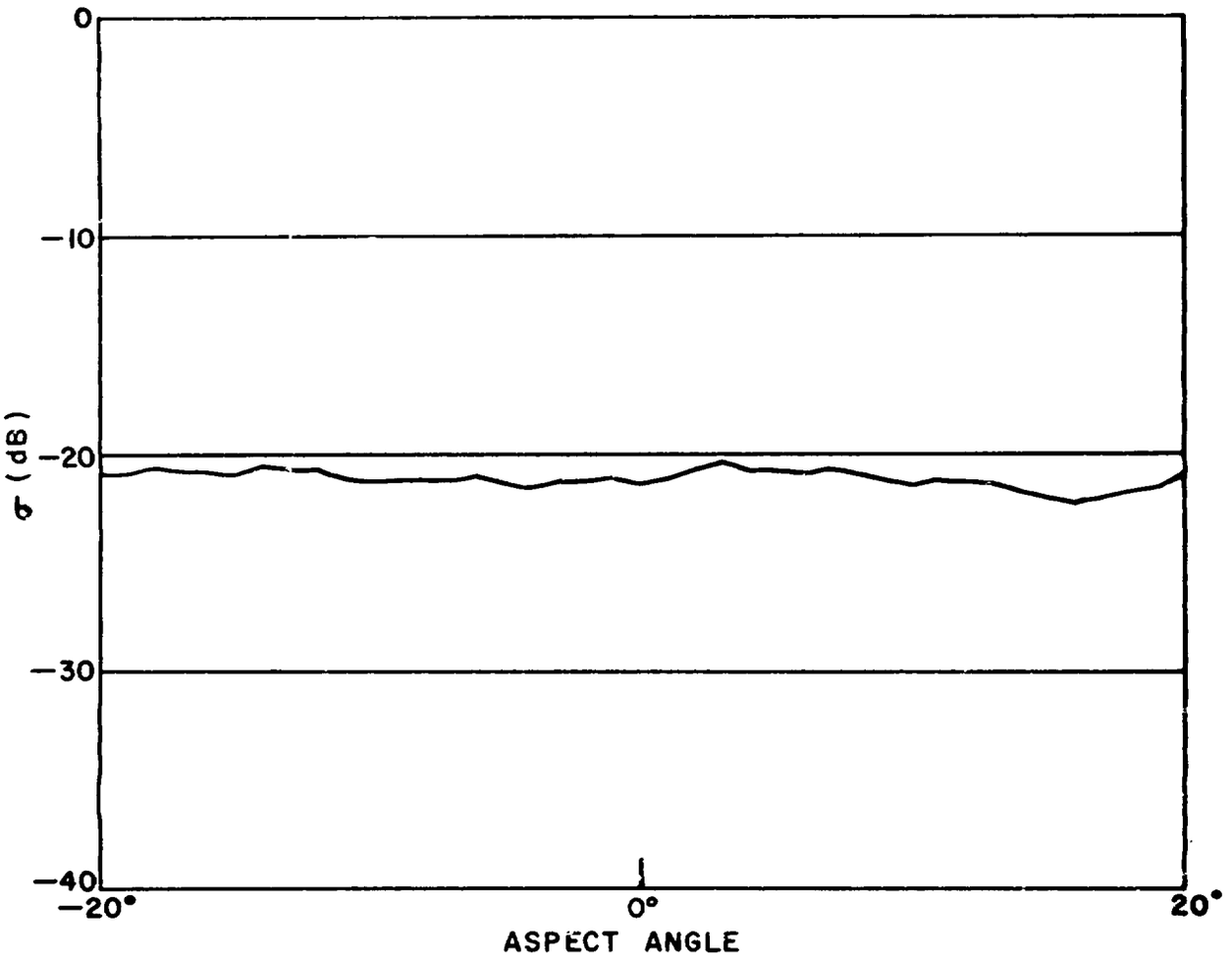

Figure 20. Smoothed and Averaged Backscatter from Nose and Tail Region of 70° Sphere-capped Cylinder (Chaff Cloud Model). f = 16 GHz.

If one accepts the broadside backscatter from a flat metallic plate as

$$\sigma_{ref} = \frac{4\pi \ell^4}{\lambda^2} ,$$

where ℓ is the side length of a square plate and λ is the wavelength, we obtain the following echo areas, σ_{ref}, for the 6 3/4" reference plate at the four frequencies of interest

f (GHz)	σ_{ref} (cm^2)	$\overline{\sigma}_{cloud}$ (cm^2)
10	120,647	1206
12	173,731	1737
14	236,468	2365
16	308,856	3089

From Figures 17-20, we see that at each frequency the average echo area of the chaff cloud at end-fire remains about 20 dB below that of the respective flat plate, these cloud echos forming the third column in the above table. This implies that the echo in cm^2 rises as the square of the frequency, as shown in Figure 21, at least in the frequency range considered.

Viewed end-on, the target appears to the eye in silhouette approximately as a 12" diameter circular flat plate. The broadside echo of such a plate, if metallic, would be about 27.9 dB above the average values measured for the target at end-fire. A smooth metallic sphere of this same diameter (12") would have an echo area of about 730 cm^2 which remains constant with increasing frequency. These relative data are presented in Figure 18.

Measurements of the dipole coated 8" circular foam disks described previously, and of a dipole-coated 6 3/4" square foam plate at 10 GHz are included as well for comparison.

It appears that, over the frequency range 10-16 GHz, the spherical cap of dipoles acted like a circular flat plate (viewed broadside) of the same diameter, but with a reflection coefficient 27.9 dB lower.

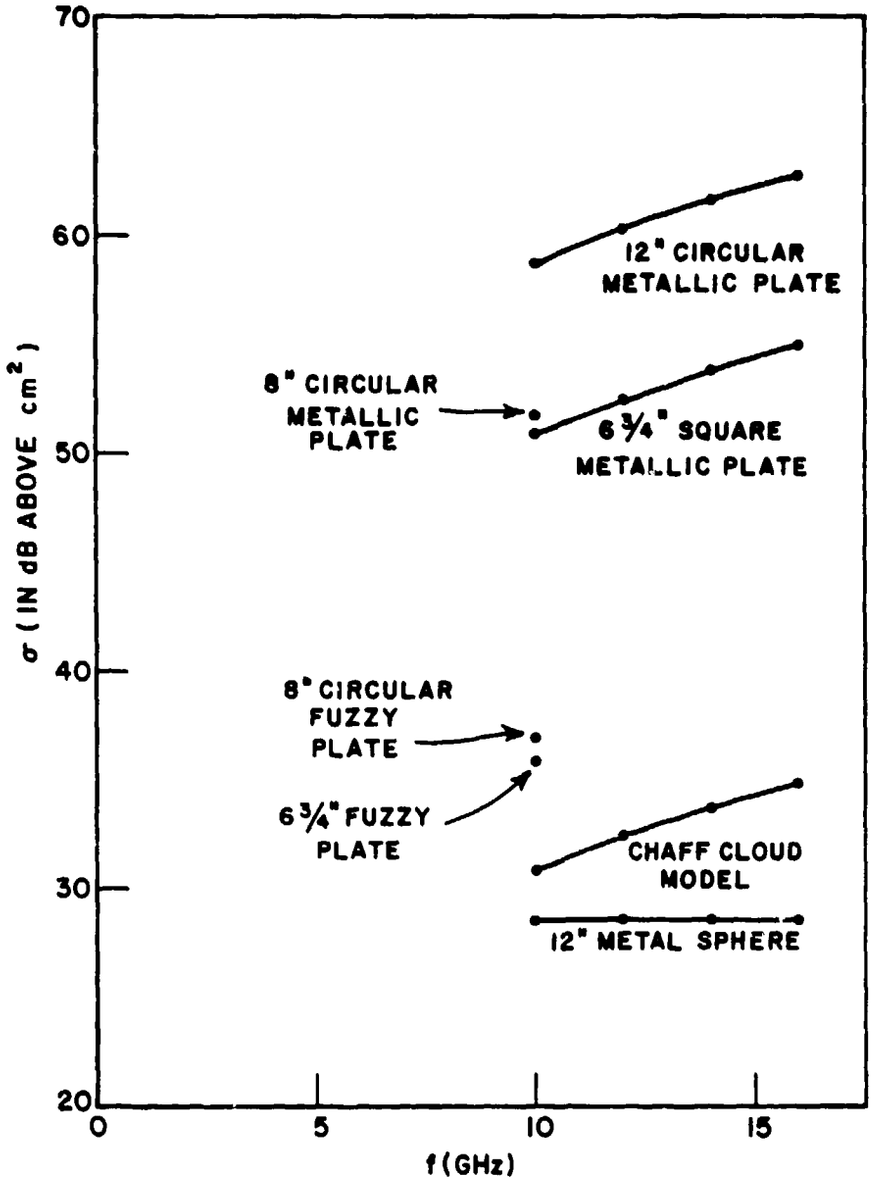

Figure 21. Relative Echo Areas of Several Obstacles.

SECTION IV
SUMMARY

A simple mathematical model (the traveling wave model) was developed which allows the incorporation of arbitrarily long, lossy, straight chaff elements into a cloud of smaller (resonant) filaments without increasing the overall size of the metrix whose inversion is necessary to obtain cloud radar cross section. In this cloud, the small filaments can be as near as $\lambda/10$ to the longer filaments, i.e., strongly coupled to the larger filaments. And the short filaments can be all coupled to each other (up to 200 such short filaments, all mutually coupled, have been considered in earlier work). But the longer filaments must be far enough away from each other so as to be decoupled from each other directly (they may be coupled to each other through the short filaments). The reason direct coupling between any two long filaments is disallowed is that the mathematical model for the current on any long filament consists of three traveling waves; the presence of another long wire in the near vicinity would disturb this current distribution to something more intricate, which could not be simply decomposed into three travelling waves. Other "modes" would have to be added, which would increase the dimension of the matrix involved, negating the advantage of the present theory. At the end of the contract period it was not clear whether the travelling wave theory could be successfully modified to accommodate coupling to nearby long filaments. It appears promising enough, however, to suggest that further effort be devoted to this problem. Certainly, for the single long filament, this very simple model has proven to be accurate.

In addition, a series of measurements of the scattering from chaff-coated foam shapes were taken to obtain estimates of the cross section of targets for which the computer model does not apply. From the polarization properties of the backscatter, it was determined that the average backscatter in other than specular regions depolarized in a fashion similar to randomly oriented dipoles.

For a target consisting of a cylinder with a spherical end cap coated with chaff dipoles (intended to represent a chaff cloud shortly after deployment), the end-on echo varied with frequency essentially as a flat plate of the same physical area, but about 27.9 dB lower in magnitude.

REFERENCES

1. R. J. Garbacz, V. Cable, R. Wickliff, R. Caldecott. J. Buk, D. Lam, K. Demarest, A. Yee, "Advanced Radar Reflector Studies," Final Report 3401-3, December 1975, The Ohio State University ElectroScience Laboratory, Department of Electrical Engineering; prepared under Contract F33615-72-C-1435 for Aeronautical Systems Division, Wright-Patterson Air Force Base, Ohio.
(AFAL-TR-75-219)

2. E. Hallen, Electromagnetic Theory, New York; John Wiley, pp. 471-493, 1962.

3. Y. M. Chen and J. B. Keller, "Current on an Input Impedance of a Cylindrical Antenna," Journal of Research NBS, Vol. 66D (Radio Prop.), No. 1, pp. 15-21, 1962.

4. J. B. Anderson, "Admittance of Infinite and Finite Cylindrical Metallic Antenna," Radio Science, Vol. 3, pp. 607-621, June 1968.

5. L. C. Shen, T. T. Wu and R. W. P. King, "A Simple Formula of Current in Dipole Antennas," IEEE Trans. Antennas Propagation, Vol. AP-16, pp. 542-547, September 1968.

6. L. C. Shen, "A Simple Theory of Receiving and Scattering Antennas," IEEE Trans. Antennas Propagation, Vol. AP-18, pp. 112-114, January 1970.

7. E. C. Jordan, Electromagnetic Waves and Radiating Systems, Englewood Cliffs, N. J., Prentice-Hall, pp. 546-549, 1950.

8. S. A. Schelkunoff and H. T. Friis, Antennas Theory and Practice, New York, John Wiley, pp. 297-298, 1952.

9. L. Solymar, "Derivation of Diffraction Coefficients for a Thin Wire of Finite Length," Electronics Letters, Vol. 9, pp. 438-440, September 1973.

10. S. W. Lee. D. C. Chang and L. Rispin, "A Simple Expression for Currents on a Finite, Thin-wire Antenna Illuminated by a Plane Wave of Arbitrary Incidence," IEEE AP-S International Symposium, pp. 181-184, October 1976.

11. J. H. Richmond and N. H. Geary, "Mutual Impedance Between Coplanar-Skew Dipoles," IEEE Trans. Antennas Propagation, Vol. AP-18, pp. 414-416, May 1970.

12. J. H. Richmond and N. H. Geary, "Mutual Impedance of Nonplanar-Skew Sinusoidal Dipoles " IEEE Trans. Antennas Propagation, Vol. AP-23, pp. 412-414, May 1975.

13. J. H. Richmond, "Computer Program for Thin-Wire Structures in a Homogeneous Conducting Medium," Report NASA-CR-2399, June 1974. For sale by National Technical Information Service, Springfield, Virginia 22161, price $3.75.

14. J. J. Bowman, T. B. A. Senior, and P. L. E. Uslenghi, Electromagnetic and Acoustic Scattering by Simple Shapes, North Holland Publishing Co., Amsterdam, pp. 472-502, 1969.

15. G. T. Ruck, D. E. Barrick, W. D. Stuart, C. K. Krichbaum, Radar Cross Section Handbook,1970.

16. E. M. Kennaugh, "Effects of the Type of Polarization on Echo Characteristics," Quarterly Progress Report 389-17, December 1952, The Ohio State University ElectroScience Laboratory, Department of Electrical Engineering; prepared under Contract AF 28(099)-90 for Rome Air Development Center. (AD 21812)

17. E. M. Kennaugh, "Effects of Type of Polarization on Echo Characteristics," Final Engineering report, Vol. I," Report 389-9, June 1951, The Ohio State University ElectroScience Laboratory, Department of Electrical Engineering; prepared under Contract AF 28(099)-90 for Rome Air Development Center. (ATI-159608)

☆U.S.Government Printing Office: 1980 — 657-084/457